A Two-Step Horizon Optimum Switching Vector - Model Predictive Control with a Novel Shunt Active Filter Reference Current Extraction Technique

Abstract:

Shunt Active Filters (SAFs) can be used for harmonic mitigation, reactive power compensation and power factor control in electrical distribution networks. Model Predictive Controller (PMC) can be used to give optimum performance for SAF's due to its inherent cost function optimization. The SAF's reference current extraction technique in Finite Control Set-Model Predictive Controller (FCS-MPC) plays a vital role in the effectiveness of the SAF's operation. The advantage of FCS-MPC is that it closely tracks the reference and injects the required compensating currents by optimizing the SAF's switching vector and it does not require an external modulator for pulse generation. FCS-MPC can be implemented as either an Optimal Switching Vector MPC (OSV-MPC) or an Optimal Switching Sequence MPC (OSS-MPC) technique. The OSV-MPC technique is simple and efficient for SAF applications. In this paper, a novel reference current extraction technique, the Inverse Matrix Average pq-SRF (IMApq-SRF) technique, is proposed along with the OSV-MPC technique. Practically a two-step delay compensation is essential in the implementation of the technique for the control of a SAF. Hence in this paper a two-step horizon OSV-MPC technique is proposed along with a IMApq-SRF reference current extraction technique to improve the power quality in distribution networks. The presented results show that the proposed methodology gives optimum SAF performance under a large range of supply and load conditions.

Keywords: Finite control set, IMApq-SRF technique, model predictive controller, optimal switching vector, shunt active filter, two step horizons

1. Introduction

The increasing use of non-linear loads on electrical distribution networks results in the generation of harmonics, excess reactive power absorption and poor power factor. Harmonic generation can lead to increased copper and iron losses, over heating of neutral conductors, malfunctioning of relays and circuit breakers, an increased kVA burden, transformer saturation, increased electrical stress on equipment and interference with telecommunication lines [1].

In distribution networks, mitigating the current harmonics is inevitable needed due to their increasing severity. Traditionally, Tuned Passive Filters (TPFs) such as single tuned, double tuned and triple tuned passive filters were being used to mitigate the lower order current harmonics [1]. TPFs are series and/or parallel connected resistance, inductance and capacitance and connected in parallel with the loads in a shunt configuration. TPFs work by using resonance between the passive components at selected harmonic frequencies. TPFs are simple in design, low cost and very efficient at mitigating lower order current harmonics. The disadvantages of TPFs are the large size, source dependent, tuning difficulties, and unsuitability for dynamic conditions and difficulty in mitigating higher order harmonics [2].

SAFs are an alternative to TPFs in electrical distribution network applications. SAFs overcome all the drawbacks of TPFs with a relatively small increment in cost compared with TPFs. The design and control of SAF is quite complex since they should meet the multiple objectives of harmonic mitigation, reactive power compensation and power factor control under a range of system conditions including steady state and transient conditions, unbalanced supply and unbalanced load conditions, and distorted supply conditions [3].

A SAF injects harmonic currents in reverse direction to the load current harmonics so that these currents cancel each other. SAFs require three main controllers, namely the reference current extraction, pulse generation and dc-link voltage regulation. All these controllers coordinate with each other to meet the SAF objectives. Many time domain reference current extraction techniques such as p-q, SRF, unit vector, synchronous detection, adaline and Icosφ techniques can be used for SAFs [3]. Each technique has its own advantages and disadvantages. The advantages of the p-q and SRF techniques can be combined to form a novel reference current extraction technique called the Apq-SRF technique. This technique gives an optimum performance under steady and transient state conditions, balanced and unbalanced supply and load conditions and distorted supply conditions [4]. This technique combines the features of both the conventional p-q and SRF techniques [4]. Similar technique such as the Inverse Matrix Average pq-SRF (IMApq-SRF) technique can be used in SAFs for All Electric Aircraft (AEA) applications [5].

Model Predictive Control (MPC) has been used to predict the future control variables one step or two steps ahead using predictive techniques and give optimised performance due to the use of a cost function. MPC can be used to control the various in many power electronic circuits [6]. Among all the proposed MPC controllers, the FCS-MPC technique is the most widely used for Voltage Source Inverter (VSI) applications [6].

The proposed two step ahead OSV-MPC technique in combination with the novel IMApq-SRF reference current extraction technique gives the robust and optimized performance in SAF's under a large range of supply and load conditions. This is the novelty of the work presented in this paper.

In this paper, Section 1 briefs the importance of harmonic mitigation, conventional harmonic mitigation techniques and a brief introduction to the MPC and IMApq-SRF technique. Various MPC techniques, block diagram of SAF with MPC technique and the mathematical modelling of IMApq-SRF technique along with liner extrapolation techniques are elaborated in Section 2. Section 3 explains the prediction of the SAF compensating currents with Forward Euler approximation. The cost function and its weighting factors are given in Section 4. Results are presented in Section 5.

2. Prediction of Reference Currents

The classification of MPC techniques is as shown in Fig.1. The FCS-MPC technique is widely used for power electronics applications. The advantage of FCS-MPC is that it works in a discrete mode and does not require an external modulator (PWM switching scheme) like some MPC strategies [6].

The OSV-MPC technique has been proved to be efficient in controlling Voltage Source Inverters (VSIs). Hence, in this paper, the OSV-MPC technique has been used along with a IMApq-SRF reference current extraction.

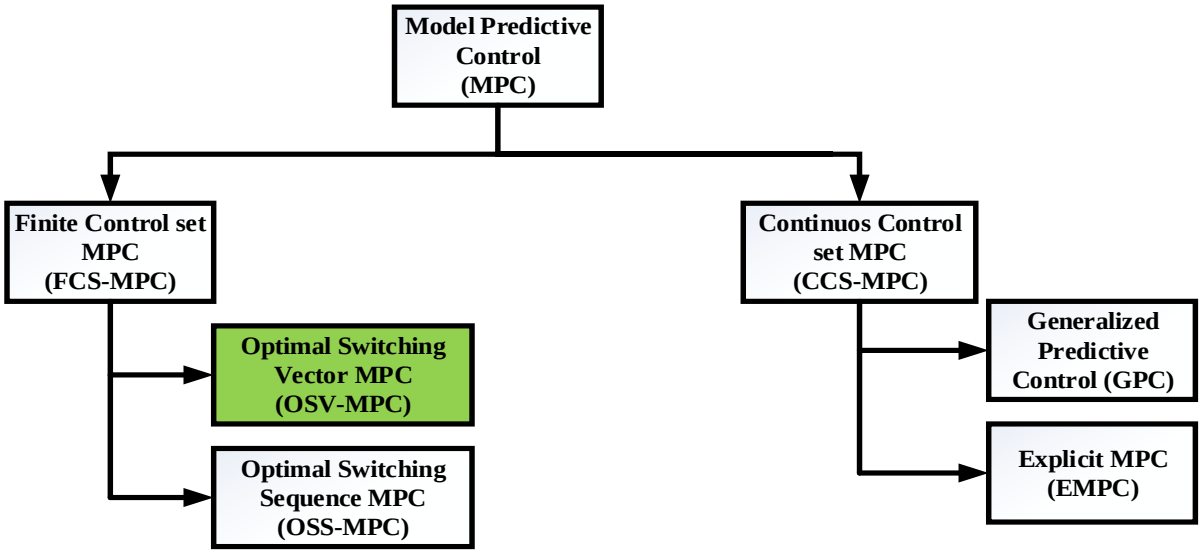

Fig.1 The MPC Classification [6]

A general block diagram of the proposed SAF with the predictor, cost function and reference current extraction is as shown in Fig.2. The IMApq-SRF reference compensating currents are extrapolated with a two-step horizon using extrapolation techniques [ref]. The SAF compensation currents are predicted for the next two sampling times using a back Euler approximation [ref]. The cost function compares the two-step ahead reference and actual SAF compensation currents. The various switching combinations involve in cost function are calculated iteratively and one combination will be selected as the optimal voltage vector for the next sampling period. The optimized voltage vector produces very small errors between references and actual values, thus giving optimizing in the SAF performance.

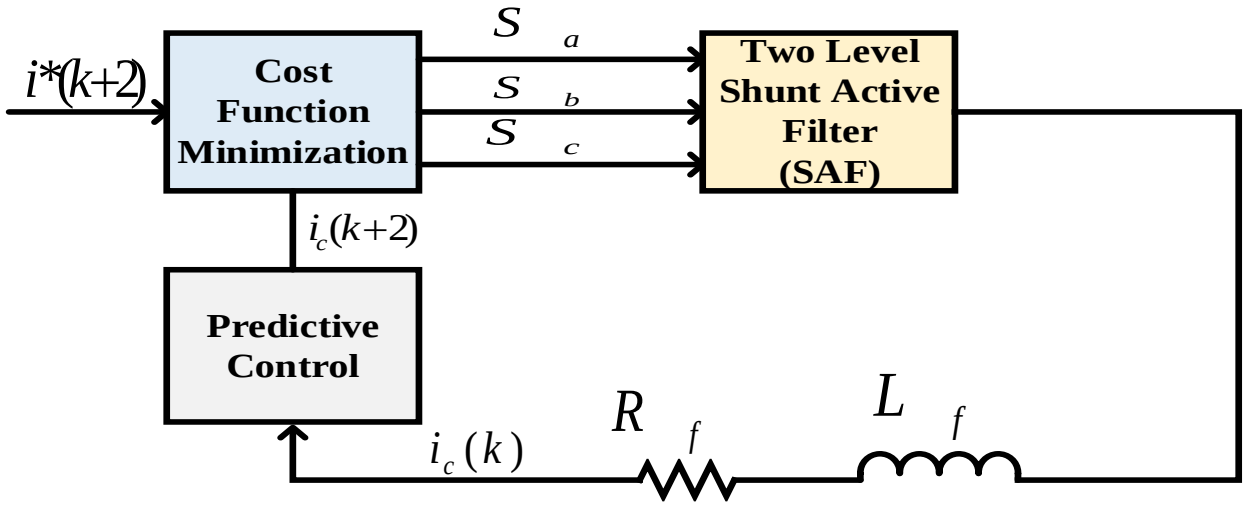

Fig.2 General Block diagram of the SAF with predictive control

The block diagram of the proposed IMApq-SRF reference current extraction technique is shown in Fig.3. The p-q and SRF theory reference currents are extracted separately and then matrix A and B derived. The inverse of matrix A and B results in the new compensating p-q and SRF currents. These new compensating currents are combined using a matrix average that gives the proposed IMApq-SRF reference currents.

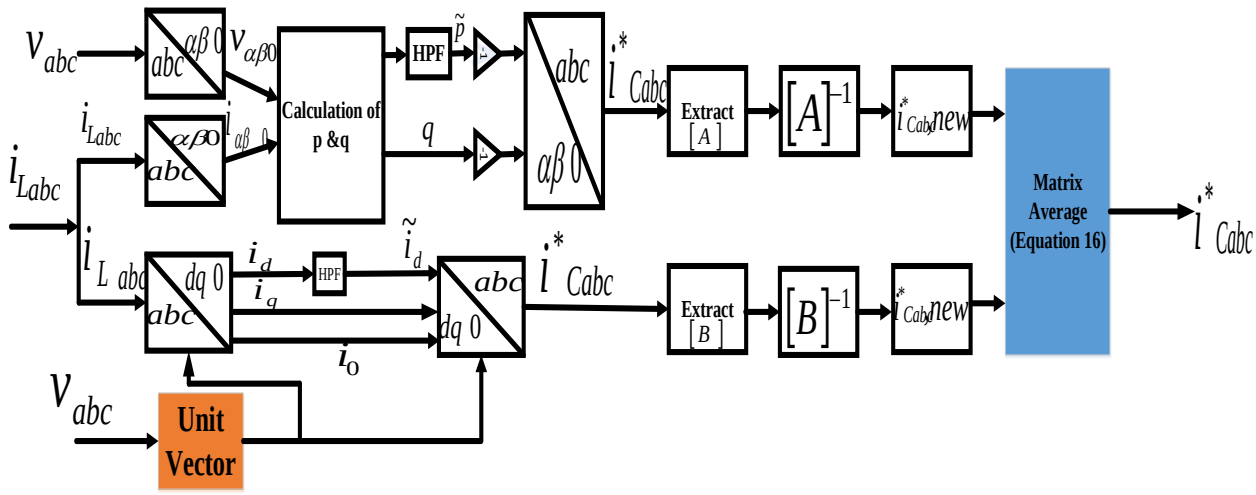

Fig.3 Block diagram of the proposed IMApq-SRF technique

The mathematical model can be formed as follows. Initially he conventional p-q theory (Clarke transformation) reference currents are found, as given in (1)

$$\begin{bmatrix} i^*_{Ca} \\ i^*_{Cb} \\ i^*_{Cc} \end{bmatrix} = \sqrt{\frac{2}{3}} \begin{bmatrix} \frac{1}{\sqrt{2}} & 1 & 0 \\ \frac{1}{\sqrt{2}} & -\frac{1}{2} & \frac{\sqrt{3}}{2} \\ \frac{1}{\sqrt{2}} & -\frac{1}{2} & -\frac{\sqrt{3}}{2} \end{bmatrix} \begin{bmatrix} -i_0 \\ i_{C\alpha} \\ i_{C\beta} \end{bmatrix} \tag{1}$$

From (1), the matrix $[A]$ can be written as given in (2)

$$[A] = \begin{bmatrix} \frac{1}{\sqrt{2}} & 1 & 0 \\ \frac{1}{\sqrt{2}} & -\frac{1}{2} & \frac{\sqrt{3}}{2} \\ \frac{1}{\sqrt{2}} & -\frac{1}{2} & -\frac{\sqrt{3}}{2} \end{bmatrix} \tag{2}$$

The disadvantage of p-q theory is that, when the grid is distorted and/or unbalanced, these reference currents are not effective in meeting the SAF objectives.

The inverse of $[A]$ is given by (3)

$$[A]^{-1} = \begin{bmatrix} 0.47 & 0.47 & 0.47 \\ 0.67 & -0.34 & -0.34 \\ 0 & 0.58 & -0.58 \end{bmatrix} \tag{3}$$

The new p-q reference current equation is given by (4) and (5)

$$\begin{bmatrix} i^{*}_{Ca,new} \\ i^{*}_{Cb,new} \\ i^{*}_{Cc,new} \end{bmatrix} = \sqrt{\frac{2}{3}}[A]^{-1} \begin{bmatrix} -i_0 \\ i_{C\alpha} \\ i_{C\beta} \end{bmatrix} \tag{4}$$

$$\begin{bmatrix} i^{*}_{Ca,new} \\ i^{*}_{Cb,new} \\ i^{*}_{Cc,new} \end{bmatrix} = \sqrt{\frac{2}{3}} \begin{bmatrix} 0.47 & 0.47 & 0.47 \\ 0.67 & -0.34 & -0.34 \\ 0 & 0.58 & -0.58 \end{bmatrix} \begin{bmatrix} -i_0 \\ i_{C\alpha} \\ i_{C\beta} \end{bmatrix} \tag{5}$$

Similarly, the reference currents in SRF control (park transformation) can be given as shown in (6)

$$\begin{bmatrix} i^{*}_{Ca} \\ i^{*}_{Cb} \\ i^{*}_{Cc} \end{bmatrix} = \sqrt{\frac{2}{3}} \begin{bmatrix} \cos\theta & -\sin\theta & 1 \\ \cos(\theta-120) & -\sin(\theta-120) & 1 \\ \cos(\theta+120) & -\sin(\theta+120) & 1 \end{bmatrix} \begin{bmatrix} \tilde{i}_d - i_{loss} \\ i_q \\ i_0 \end{bmatrix} \tag{6}$$

The drawback of SRF theory is that it does not have any relationship for reactive power compensation, thus it fails to meet the ideal SAF objectives.

From (6), The matrix $[B]$ can be found from (7)

$$[B] = \begin{bmatrix} \cos\theta & -\sin\theta & 1 \\ \cos(\theta-120) & -\sin(\theta-120) & 1 \\ \cos(\theta+120) & -\sin(\theta+120) & 1 \end{bmatrix} \tag{7}$$

The inverse of $[B]$ can be found using (8)

$$[B]^{-1} = \frac{2}{3} \begin{bmatrix} \cos\theta & \cos(\theta-120) & \cos(\theta-240) \\ -\sin\theta & -\sin(\theta-120) & -\sin(\theta-240) \\ 0.5 & 0.5 & 0.5 \end{bmatrix} \tag{8}$$

The new SRF reference currents are then given by (9) and (10)

$$\begin{bmatrix} i^{*}_{Ca,new} \\ i^{*}_{Cb,new} \\ i^{*}_{Cc,new} \end{bmatrix} = \sqrt{\frac{2}{3}}[B]^{-1} \begin{bmatrix} \tilde{i}_d - i_{loss} \\ i_q \\ i_0 \end{bmatrix} \tag{9}$$

$$\begin{bmatrix} i^{*}_{Ca,new} \\ i^{*}_{Cb,new} \\ i^{*}_{Cc,new} \end{bmatrix} = \frac{2}{3}\sqrt{\frac{2}{3}} \begin{bmatrix} \cos\theta & \cos(\theta-120) & \cos(\theta-240) \\ -\sin\theta & -\sin(\theta-120) & -\sin(\theta-240) \\ 0.5 & 0.5 & 0.5 \end{bmatrix} \begin{bmatrix} \tilde{i}_d - i_{loss} \\ i_q \\ i_0 \end{bmatrix} \tag{10}$$

The matrix averaging of (5) & (10) gives the novel IMApq-SRF reference current extraction technique, as represented in (11)

$$\begin{bmatrix} i^*_{Ca,new} \\ i^*_{Cb,new} \\ i^*_{Cc,new} \end{bmatrix} = \sqrt{\frac{2}{3}} \begin{bmatrix} 0.47i_{c\alpha} + 0.47i_{c\beta} + 0.67(\tilde{i}_d - i_{loss})\cos\theta + 0.67i_q\cos(\theta - 120) + 0.67i_0(\cos(\theta - 240) - 0.47) \\ -0.34i_{c\alpha} - 0.34i_{c\beta} - 0.67(\tilde{i}_d - i_{loss})\sin\theta - 0.67i_q\sin(\theta - 120) - 0.67i_0(1 + \sin(\theta - 240)) \\ 0.58i_{c\alpha} - 0.34i_{c\beta} + 0.34(\tilde{i}_d - i_{loss}) + 0.34i_q + 0.34i_0 \end{bmatrix} \quad (11)$$

Equation (11) gives the advantages of conventional p-q and SRF techniques and therefore makes the proposed SAF more robust under all practical conditions.

For small sampling times, the predicted reference current is almost equal to actual current, whereas for large sampling times, extrapolation is required to predict the one-step or two-step ahead values of currents [7]. A simple solution is to apply a linear extrapolation to predict the reference current to the next two sampling instants with the present and previous reference values [8].

Fig.4 Extrapolation of reference currents

The error vector can be given by (12)

$$\begin{aligned} \Delta(i_q + i_{c\beta})/2 &= -\sum_{m=1,2}[2C'_m C_m(i_q + i_{c\beta})/2 + 2S'_m S_m(i_q + i_{c\beta})/2] \\ \Delta(i_d + i_{c\alpha})/2 &= \sum_{m=1,2}[2C'_m C_m(i_d + i_{c\alpha})/2 + 2S'_m S_m(i_d + i_{c\alpha})/2] \end{aligned} \quad (12)$$

The one-step ahead predicted reference currents can be found using (13)

$$i^*_{c(k+1)} = \frac{(i_q + i_{c\beta})/2\Delta(i_q + i_{c\beta})/2 + +(i_d + i_{c\alpha})/2\Delta(i_d + i_{c\alpha})/2}{2} \quad (13)$$

The two step ahead horizon predicted reference currents can then be found using (14)

$$i^*_{c(k+2)} = i^*_{c(k+1)} + \Delta i_{c(k+1)} \quad (14)$$

Where

$$\begin{aligned} C_m &= \cos 6m\theta \\ S_m &= \sin 6m\theta \\ C'_m &= \cos 6m\theta - \cos 6m(\theta + \theta_s) \\ S'_m &= \sin 6m\theta - \sin 6m(\theta + \theta_s) \\ \theta &= \omega T_s, T_s = 1/f_s \end{aligned}$$

3. Prediction of SAF Compensating Currents

A block diagram of the SAF configuration is shown in Fig.5. The two level-VSI has six IGBT switches. In each leg, the two switches are controlled in a complimentary way.

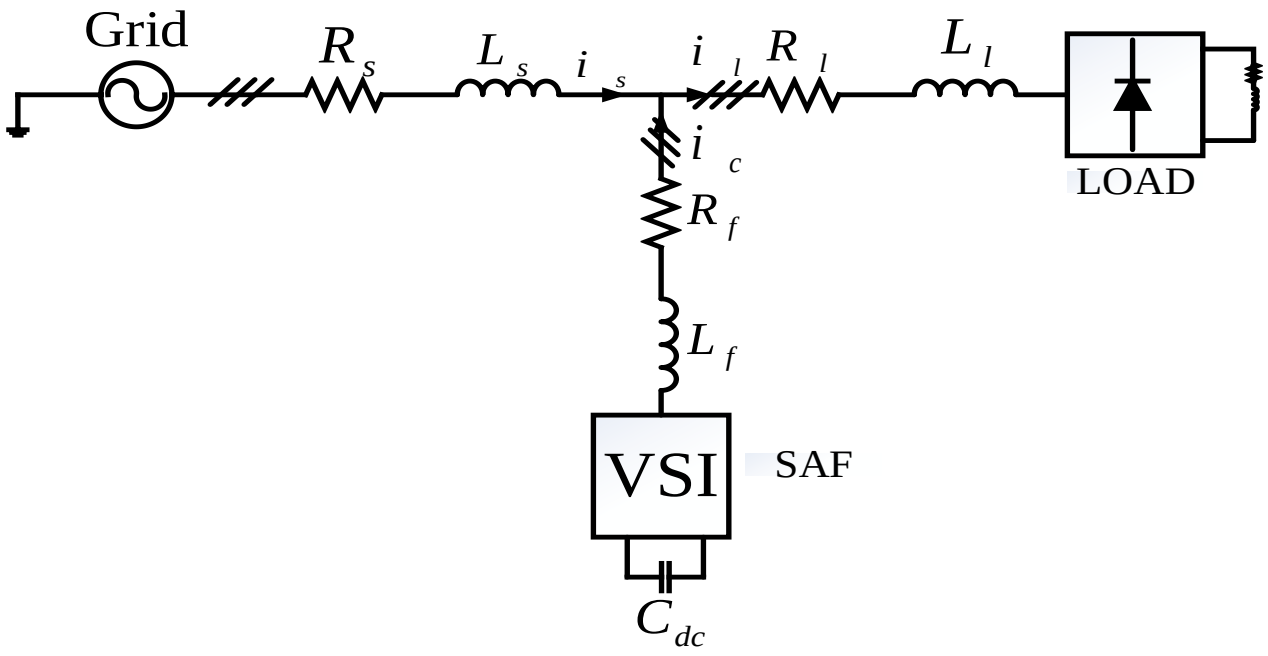

Fig.5 SAF configuration

The voltages in each phase of the leg are given by (15)

$$\begin{aligned} v_{aN} &= S_a V_{dc} \\ v_{bN} &= S_b V_{dc} \\ v_{cN} &= S_c v_{dc} \end{aligned} \tag{15}$$

v_{dc} is the VSI capacitor voltage. Considering the abc frame of 120 degrees. The output voltage vector can be calculated using (16)

$$v = \frac{2}{3}\left(v_{aN} + a v_{bN} + a^2 v_{cN}\right) \tag{16}$$

The load currents may be written as in (17), from the analysis of the circuit shown in Fig.5

$$i_l = i_s + i_c \tag{17}$$

The capacitor current that is responsible for charging and discharging is given by (18)

$$i_{dc} = i_{ca} S_a + i_{cb} S_b + i_{cc} S_c \tag{18}$$

Applying KVL to the circuit shown in Fig.5 gives the following (19)

$$L_c \frac{dic}{dt} = v - V_s - R_c i_c \tag{19}$$

The output voltages of the inverter may rewritten as (20)

$$v = V_{dc}.H.S_{abc} \tag{20}$$

Where V_{dc} is the dc- link voltage and H is the constant matrix as given by (21)

$$H = \begin{bmatrix} \frac{2}{3} & \frac{-1}{3} & \frac{-1}{3} \\ \frac{-1}{3} & \frac{2}{3} & \frac{-1}{3} \\ \frac{-1}{3} & \frac{-1}{3} & \frac{2}{3} \end{bmatrix} \tag{21}$$

There are eight possible switching combinations. Each possible switching combination generates a voltage vector. For switching sequence-1 (0, 0, 0) and the switching sequence-8, the output voltage of inverter in each phase is zero. So the switching sequence-1 & 6 is same and are not considered in this example. The switching sequence (1, 1, 0) provides an optimized vector with very less error between reference and compensating SAF currents [9]. Table I shows the possible switching states and voltage vectors

Table I Switching states and vectors

Seq. No.	S_a	S_b	S_c	v_a	v_b	v_c
1	0	0	0	0	0	0
2	0	0	1	$\frac{-V_{dc}}{3}$	$\frac{-V_{dc}}{3}$	$\frac{2V_{dc}}{3}$
3	0	1	0	$\frac{-V_{dc}}{3}$	$\frac{2V_{dc}}{3}$	$\frac{-V_{dc}}{3}$
4	0	1	1	$\frac{-2V_{dc}}{3}$	$\frac{V_{dc}}{3}$	$\frac{V_{dc}}{3}$
5	1	0	0	$\frac{2V_{dc}}{3}$	$\frac{-V_{dc}}{3}$	$\frac{-V_{dc}}{3}$
6	1	0	1	$\frac{V_{dc}}{3}$	$\frac{-2V_{dc}}{3}$	$\frac{V_{dc}}{3}$
7	**1**	**1**	**0**	$\frac{V_{dc}}{3}$	$\frac{V_{dc}}{3}$	$\frac{-2V_{dc}}{3}$
8	1	1	1	0	0	0

The two steps ahead predicted SAF compensating currents are obtained by the forward Euler approximation and is given by (22)

$$\frac{di_c}{dt} \approx \frac{i_c(k+1) - i_c(k)}{T_s} \tag{22}$$

From (19)

$$\frac{di_c}{dt} = \frac{v - V_s - R_c i_c}{L_c} \tag{23}$$

Substitute (23) in (22), gives the one-step ahead predicted SAF compensating current and is given by (24)

$$i_c(k+1) = T_s \frac{v(k) - V_s(k)}{L_c} + (1 - \frac{R_c T_s}{L_c}) i_c(k) \tag{24}$$

Similarly, the two-steps ahead predicted SAF compensating current is given by (25)

$$i_c(k+2) = T_s \frac{v(k+1) - V_s(k+1)}{L_c} + (1 - \frac{R_c T_s}{L_c}) i_c(k+1) \tag{25}$$

4. Proposed cost function

The cost function of the proposed SAF configuration is as shown in Fig.6. A two step ahead cost function is proposed for better tracking of compensation currents with reference currents. Weighing factors are also included in the cost function to control the other desired parameters.

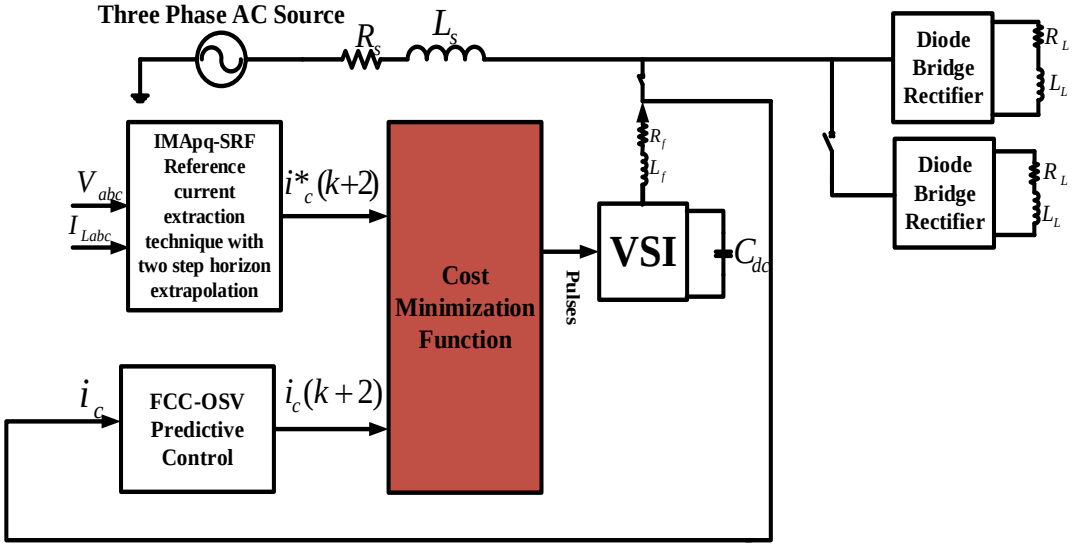

Fig.6 Cost minimization function

For OSV-MPC control strategy, the best suitable two step ahead cost function is given by (26)

$$g = \left(i_c(k+2) - i_c^*(k+2)\right)^2 + \lambda n_c \tag{26}$$

$i_c(k+2)$ - Two-step ahead SAF compensating currents

$i_c^*(k+2)$ - Two-step ahead reference compensating currents

λ - weighting factors

Weighting factors are used to combine the remaining variables apart from predicted and reference currents involved in the SAF operation. Hence, the cost function can be divided into two types, one is cost function to optimize the references (g_1), giving zero error between actual and references compensating currents, and the second is the cost function

to optimize the remaining parameters (g_2) [10]-[18]. The complete cost function can be represented by (27)

$$g = g_1 + g_2 \tag{27}$$

Where g_1 is given by (28)

$$g_1 = \left(i_c(\hat{k}+2) - i_c^*(k+2) \right)^2 \tag{28}$$

Where g_2 is as shown in (29) and (30)

$$g_2 = \lambda n_c \tag{29}$$

$$g_2 = \lambda_1 n_{c1} + \lambda_2 n_{c2} + \lambda_3 n_{c3} \tag{30}$$

$\lambda_1, \lambda_2 \,\&\, \lambda_3$ are the weighting factors. $\lambda_3 = 1$; This is always constant. $\lambda_2 \,\&\, \lambda_3$ values are adjusted according to the system conditions and variations.

Where

$$\begin{aligned} n_{c1} &= \frac{1}{V_{dc,reted}} \left| V^*_{dc}(k+2) - V_{dc}(k+2) \right| \\ n_{c2} &= \frac{1}{P_{s,rated}} \left| P_s^*(k+2) - P_s(k+2) \right| \\ n_{c3} &= \frac{1}{P_{s,rated}} \left| Q_s^*(k+2) - Q_s(k+2) \right| \end{aligned} \tag{31}$$

5. Results

The proposed system was modelled with various blocks of MATLAB Simulink software. Initially, a three phase distribution network with one fixed uncontrolled bridge rectifier and one variable uncontrolled bridge rectifier (turned on at time t=0.5 sec) was modelled to create a highly polluted distorted supply voltage and load current. After measuring the THD, the proposed SAF configuration was modelled and connected at the PCC to test its performance under a large range of supply and load conditions.

The load current connecting the SAF is as shown in Fig.7. The load current is highly distorted and non-sinusoidal. The THD of load current under fixed loading condition is 28.03%. The THD at dynamic loading condition is (when second load is switched on at 0.5 sec) is 28.12%.

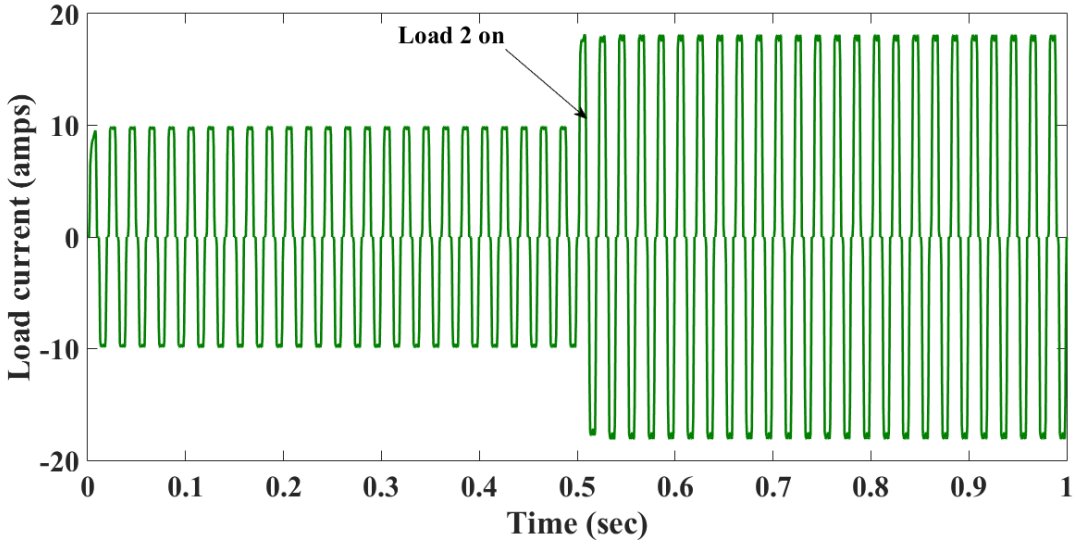

Fig.7 phase A load current without SHAF

If the SAF is turned on at 0.1 sec, the load or source current becomes sinusoidal as shown in Fig.8. The SAF injects compensating currents (I_c) in counter clock wise with respect to the harmonics present by the load current, as shown in Fig.9. Thus the load current therefore becomes sinusoidal. The SAF is able to mitigate the current harmonics under both steady state and dynamic loading conditions.

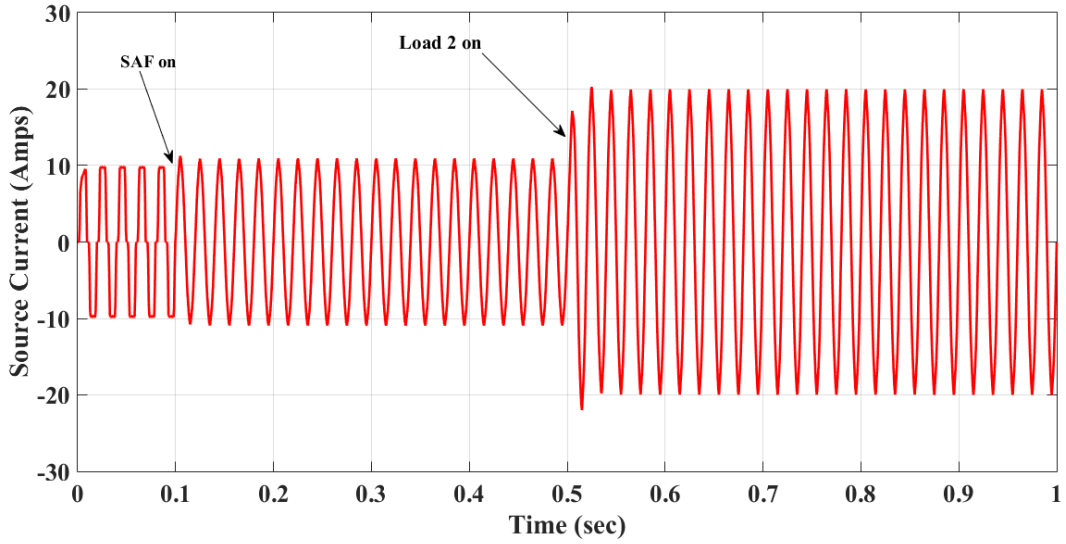

Fig.8 The source current when SAF is on at t=0.1 sec

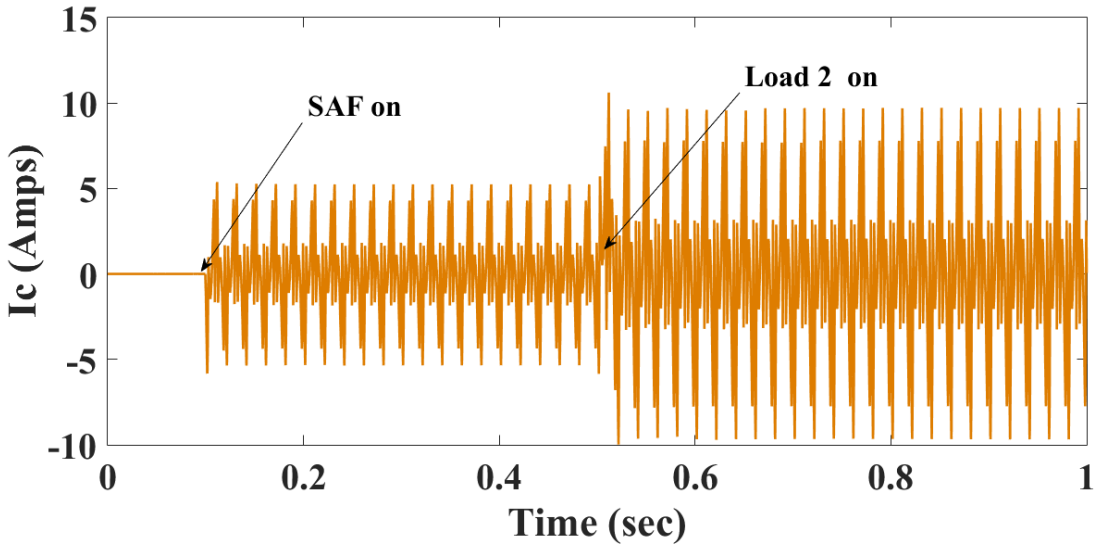

Fig.9 SAF compensating currents

The SAF control can meet multiple objectives simultaneously. The SAF is able to reduce the oscillations in real power demands, as shown in Fig.10, and is able to reduce the reactive power demand, as shown in Fig.11. The power factor correction using the SAF is shown in Fig.12.

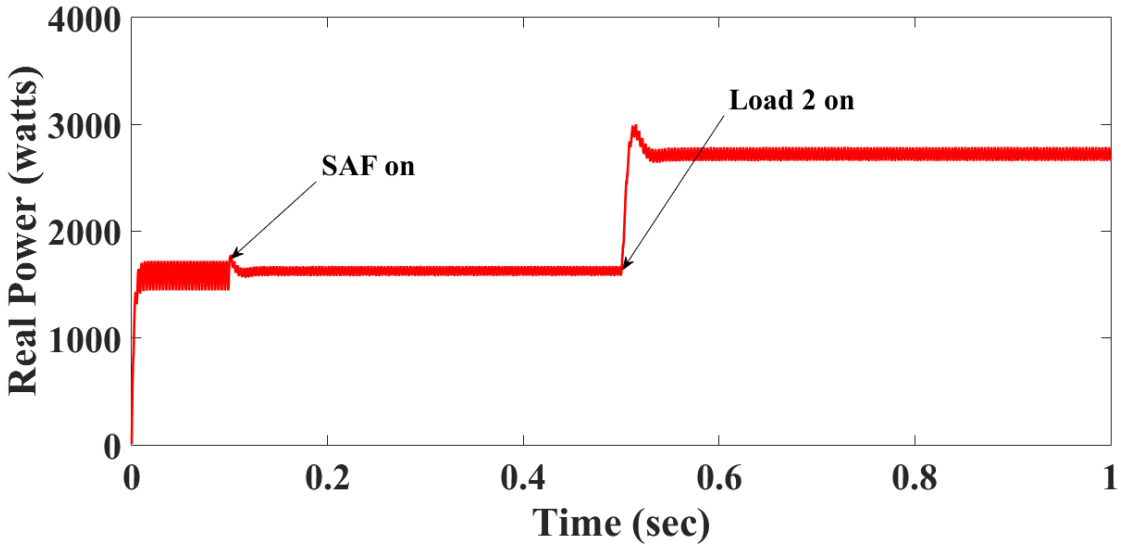

Fig.10 Reduction of real power oscillations by SAF

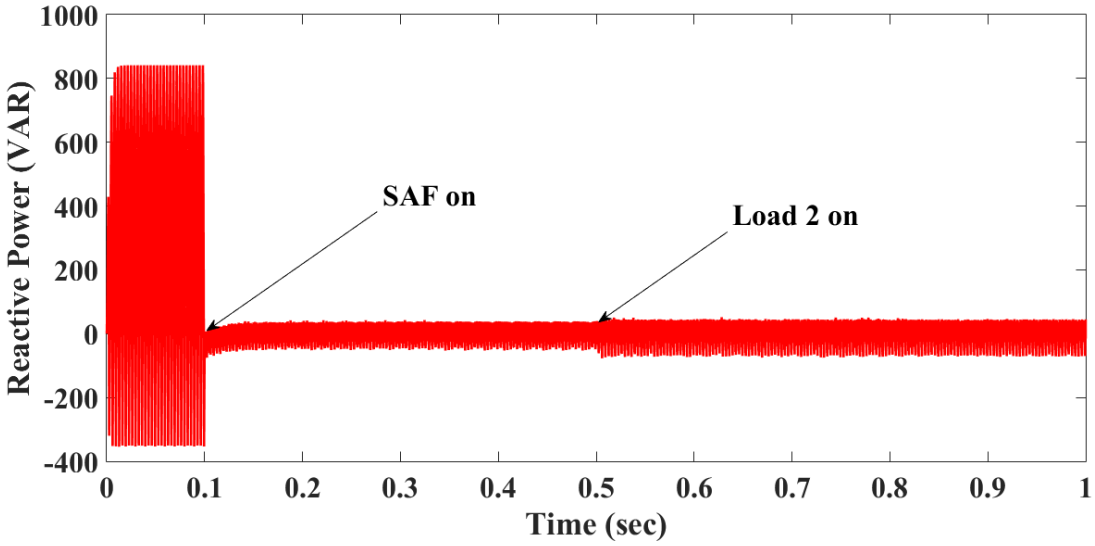

Fig.11 Reduction of reactive power demand by SAF

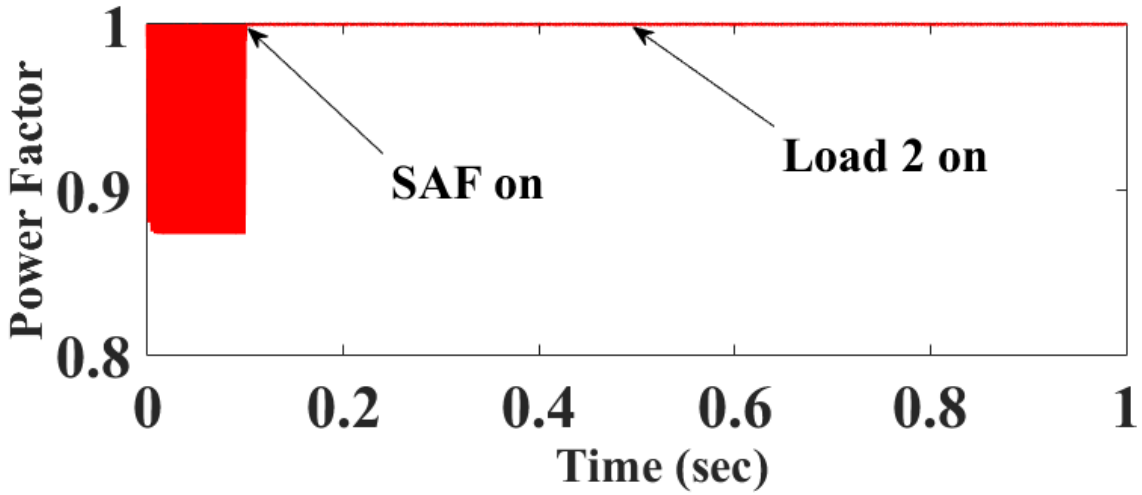

Fig.12 Power factor correction by SAF

The SAF is able to maintain constant DC link voltage (V_{dc}) is as shown in Fig.13. The DC link voltage is approximately equal to its reference level. The cost function in SAF is able to maintain zero error between actual and reference dc-link voltage by optimizing the SAF voltage vectors with two-step ahead horizon prediction.

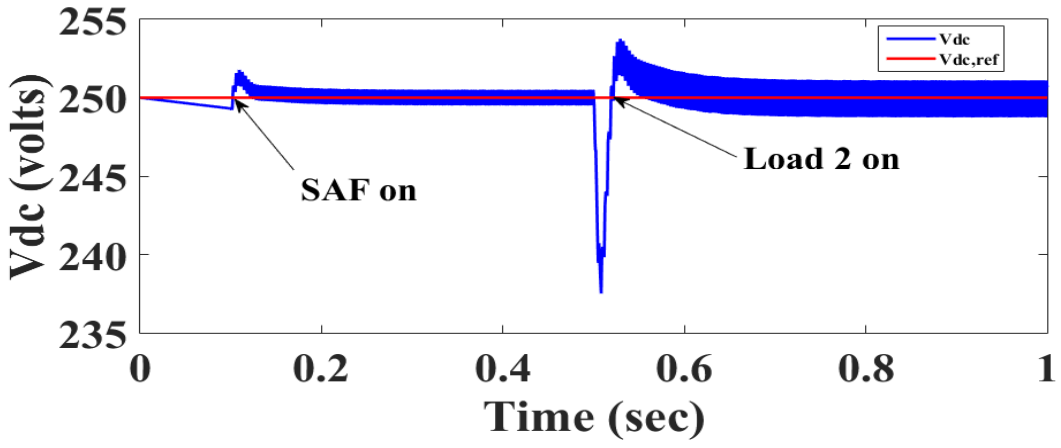

Fig.13 DC link voltage across the VSI capacitor

The main advantage of OSV-MPC is that it very closely tracks the reference ($I_{c,\,ref}$) and actual compensating currents (I_c) with near zero error, as shown in Fig.14. Thus the SAF performance is optimal.

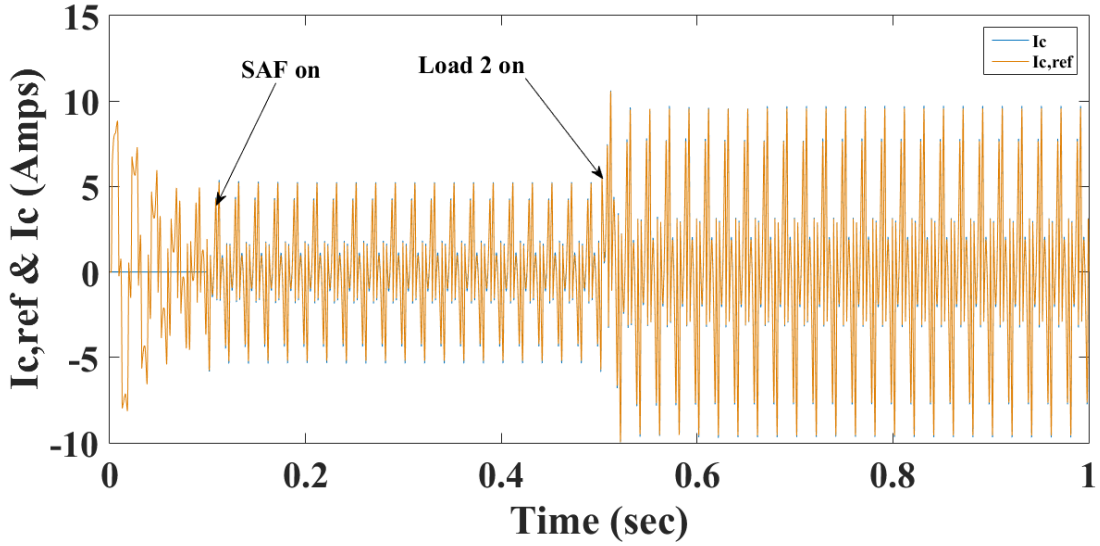

Fig.14 Reference and actual SAF compensating currents tracking

The source voltage for phase A is shown in Fig.15. The source voltage is sinusoidal throughout the SAF operation.

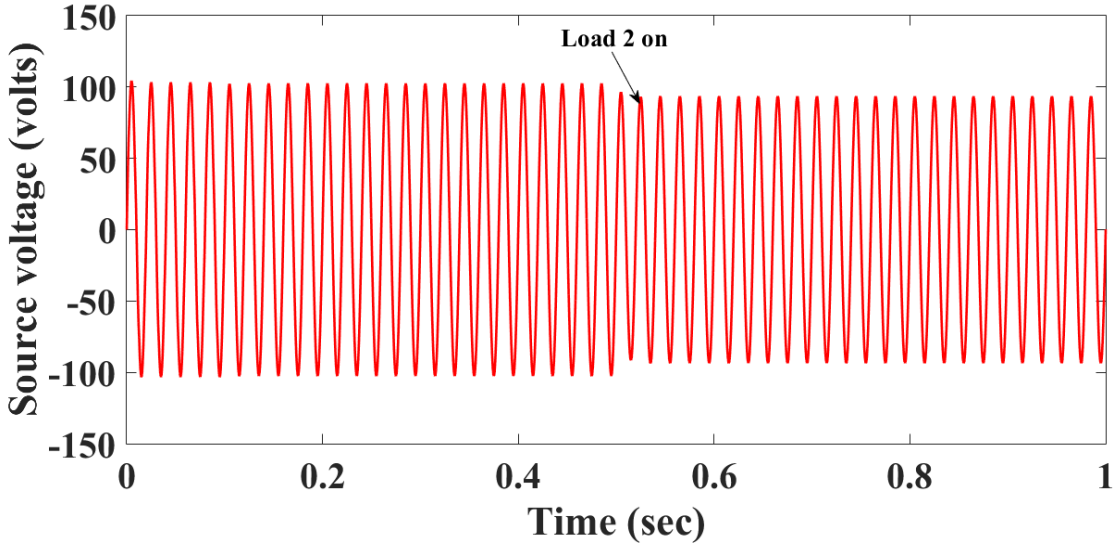

Fig.15 Source voltage of phase A

The THD of the source current with proposed SAF compensation under the fixed loading is 1.80% while under the dynamic loading condition is 1.84% as shown in Fig.16 and 17.

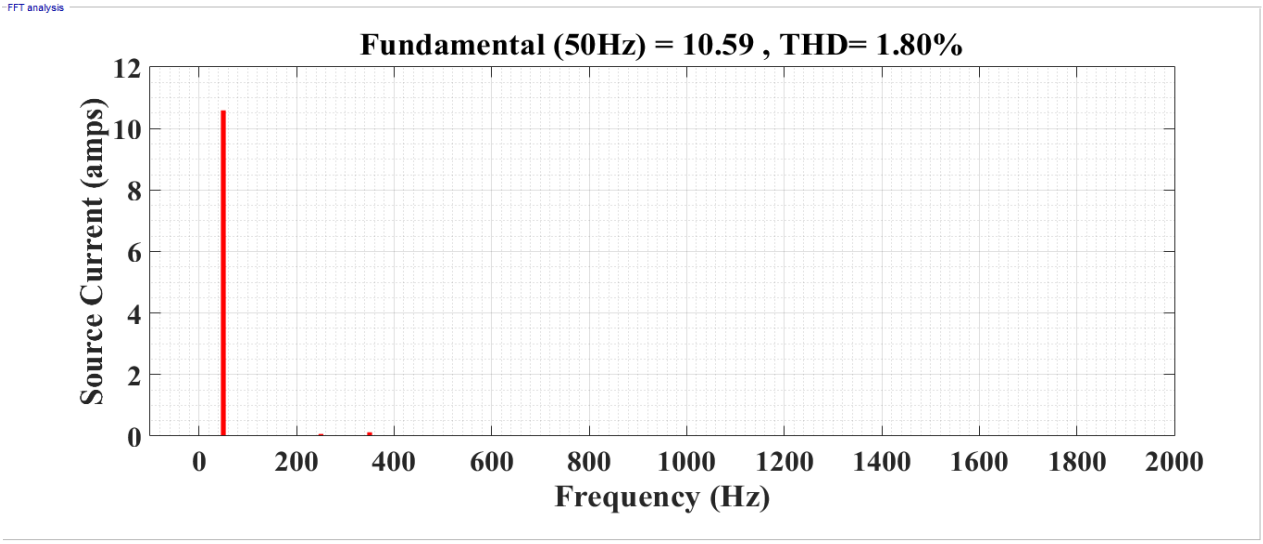

Fig.16 THD of source current with SAF compensation under fixed loading condition

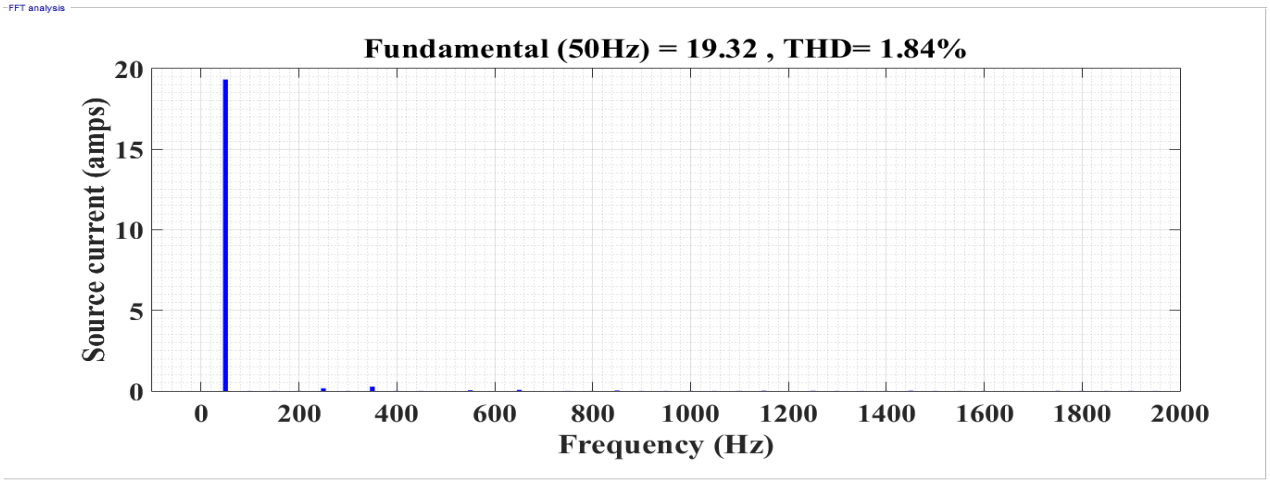

Fig.17 THD of source current with SAF compensation under dynamic condition

The comparison of the proposed SAF operation with IMApq-SRF technique and two step horizon FCS-MPC techniques is shown in Table II. Table II shows that the proposed methodology gives the optimum SAF performance by the way of excellent tracking between actual and reference compensation currents.

Table II Comparison of FCS-MPC with other conventional techniques

Type of SAF control	**THD**		**Tracking**
	Steady State	**Transient State**	
Conventional p-q theory without any MPC	2.6	2.68	Average
Conventional SRF theory without any MPC	2.2	2.31	Average
Apq-SRF theory without any MPC	1.92	2.15	Good
IMApq-SRF without any MPC	1.9	1.95	Good
The proposed IMApq-SRF with FCS-MPC	1.80	1.84	Excellent

6. Conclusions

The OSV-MPC technique with a two-step ahead prediction technique provides more robustness in the SAF operation. The SAF control is able to optimize the performance by reducing the error in its cost function. The OSV-MPC accurately tracks the reference and actual compensating currents, thus optimizing the SAF performance with less power loss. Further, the IMAPQ-SRF reference current extraction technique has been shown to have additional advantages, because of its multi-functional capability.

References:

[1] Roger C. Dugan, Mark F. Mc Granaghan, Surya Santoso and H. Wayne Beaty, *Electrical Power Systems Quality*, 2nd edition. McGraw – Hill, 2002, pp. 168–172.

[2] Cheepati, K. R, Ali. S & Kalavathi. S .M. "Overview of Double Tuned Harmonic Filters in Improving Power Quality under Non Linear Load Conditions*". International Journal of Grid and Distributed Computing*, vol.10, no.7, pp.11-26, 2017.

[3] S. F. Mekhamer, A. Y. Abdelaziz Sherif M. Ismael "Technical Comparison of Harmonic Mitigation Techniques for Industrial Electrical Power Systems" *Proceedings of the 15th International Middle East Power Systems Conference (MEPCON'12), Alexandria University, Egypt*, December 23-25, 2012, Paper ID 214.

[4] Cheepati, Kumar Reddy, Nageswara Rao Maddala, and Surya Kalavathi Munagala. "A Novel Reference Current Extraction Technique with Multi-Functional Capability for Shunt Active Filter." *Journal of Electrical Engineering & Technology*, vol.15, no.2 pp. 657-672, 2020.

[5] Kumar Reddy Cheepati, Nageswara Rao Maddala & Surya Kalavathi Munagala "A hybrid reference current extraction technique with multi-functional capability for shunt active filter in all-electric aircraft" *International Journal of Ambient Energy*, March, 2020.

[6] Sergio Vazquez, Jose Rodriguez, Marco Rivera, Leopoldo G. Franquelo and Margarita Norambuena "Model Predictive Control for Power Converters and Drives: Advances and Trends, *IEEE Transactions on Industrial Electronics*, vol. 64, no. 2, pp.935-947, 2017.

[7] Venkata Krishna Gonuguntala, Anke Fröbel, Ralf Vick "Performance Analysis of Finite Control Set Model Predictive Controlled Active Harmonic Filter" *European Union*, 2018.

[8] Seung-Gi Jeong and Myung-Ho Woo "DSP-Based Active Power Filter with Predictive Current Control" *IEEE Transactions on Industrial Electronics*, vol. 44, no. 3, pp.329-336, June, 1997.

[9] Jose Rodriguez and Patricio Cortes "Predictive Control of Power Converters and Electrical Drives", *IEEE Wiley, 1st edition*, 2012.

[10] Pericle Zanchetta, Patricio Cortes, Marcelo Perez, Jose Rodriguez and Cesar Silva "Finite States Model Predictive Control for Shunt Active Filters", *IEEE conference*,

pp.581-586, 2011

[11] J. Zhang, K. Yu, Z. Wen, X. Qi and A. K. Paul, "3d reconstruction for motion blurred images using deep learning-based intelligent systems," Computers, Materials & Continua, vol. 66, no.2, pp. 2087–2104, 2021

[12] K. Yu, L. Tan, L. Lin, X. Cheng, Z. Yi and T. Sato, "Deep-Learning-Empowered Breast Cancer Auxiliary Diagnosis for 5GB Remote E-Health," in *IEEE Wireless Communications*, vol. 28, no. 3, pp. 54-61, June 2021, doi: 10.1109/MWC.001.2000374.

[13] K. Yu, Z. Guo, Y. Shen, W. Wang, J. C. -W. Lin and T. Sato, "Secure Artificial Intelligence of Things for Implicit Group Recommendations," in *IEEE Internet of Things Journal*, doi: 10.1109/JIOT.2021.3079574

[14] K. Yu, M. Arifuzzaman, Z. Wen, D. Zhang and T. Sato, "A Key Management Scheme for Secure Communications of Information Centric Advanced Metering Infrastructure in Smart Grid," in *IEEE Transactions on Instrumentation and Measurement*, vol. 64, no. 8, pp. 2072-2085, Aug. 2015, doi: 10.1109/TIM.2015.2444238.

[15] C. Feng *et al*., "Efficient and Secure Data Sharing for 5G Flying Drones: A Block chain-Enabled Approach," in *IEEE Network*, vol. 35, no. 1, pp. 130-137, January/February 2021, doi: 10.1109/MNET.011.2000223

[16] H. Li, K. Yu, B. Liu, C. Feng, Z. Qin and G. Srivastava, "An Efficient Ciphertext-Policy Weighted Attribute-Based Encryption for the Internet of Health Things," in *IEEE Journal of Biomedical and Health Informatics*, doi: 10.1109/JBHI.2021.3075995.

[17] L. Zhen, A. K. Bashir, K. Yu, Y. D. Al-Otaibi, C. H. Foh and P. Xiao, "Energy-Efficient Random Access for LEO Satellite-Assisted 6G Internet of Remote Things," in *IEEE Internet of Things Journal*, vol. 8, no. 7, pp. 5114-5128, 1 April1, 2021, doi: 10.1109/JIOT.2020.3030856

[18] L. Zhen, Y. Zhang, K. Yu, N. Kumar, A. Barnawi and Y. Xie, "Early Collision Detection for Massive Random Access in Satellite-Based Internet of Things," in *IEEE Transactions on Vehicular Technology*, vol. 70, no. 5, pp. 5184-5189, May 2021, doi: 10.1109/TVT.2021.3076015.

Appendix:

The Simulation Parameters of the proposed system are given in Table III

Table III Simulation Parameters

Grid	V_{rms}=70 v, f = 50 Hz
Load	L_1 = 20 mH, R_1 = 20 $ohms$
	L_2 = 2 mH, R_2 = 2.5 $ohms$
VSC	C = 1100μF, L_f = 8 mH, R_f = 2.5 ohms
DC Voltage Regulator	Vdc_{ref} = 300v K_p = 0.48, K_i = 65.8
Sample time	T = 6*10^{-5} sec